Experimental Determination of UWB Ranging Errors in an Outdoor Environment

V. Kristem, S. Niranjayan, *Member, IEEE*, S. Sangodoyin, *Student Member, IEEE*, A. F. Molisch, *Fellow, IEEE*

Abstract—Ultra-wideband (UWB) technology is a good candidate to provide accurate position information indoors and in dense urban environments where Global Positioning System (GPS) is usually not reliable. This paper provides the results of a UWB ranging measurement campaign carried out in a dense urban environment. Measurements were taken with two different antenna heights in line-of-sight (LOS) and non-line-of-sight (NLOS) conditions. It is observed that the ranging errors increases when the antennas are closer to the ground, and is more significant in NLOS conditions. Also, in NLOS conditions ranging errors of more than 10 meters were observed when the LOS component is completely blocked by a building. Errors of such magnitude are typically not captured by IEEE 802.15.4a CM6 (outdoor NLOS) channel model. Since the conventional thresholding schemes provide bad ranging accuracy in presence of multiuser interference (MUI), we propose a nonlinear processing scheme of time-hopping impulse radio (TH-IR) and apply it to our measurements to show that it gives much better ranging accuracy.

I. INTRODUCTION

Accurate position information is of high importance in many commercial, public safety, and military applications. GPS provides a good position estimate when there is a good line-of-sight (LOS) to the GPS satellites. However, in indoor and dense urban environments, geolocation has always been a more challenging problem as GPS signals are not strong enough to penetrate through most materials. Thus localization based on ranging between ground-based devices becomes an attractive alternative. In particular, ranging using ultra-wideband (UWB) signals is promising due to the good range resolution associated with large bandwidth.

UWB ranging in indoor environment has been studied extensively in the literature–numerous measurement campaigns were carried out that characterized the ranging error in LOS and NLOS conditions [3]–[5] and several receiver algorithms for range extraction are proposed and analyzed in [2] and references therein. However, there are much fewer such measurements in outdoor environments (Ref. [7]), which are important for military applications, wireless sensor networks, and localization for rescue workers in disaster relief zones. Furthermore, none of the existing measurements studies the impact of antenna height on the ranging error, though the dependence of propagation conditions on height (see, e.g., [1]) suggest that such a dependence could be important.

To close this gap, we performed a ranging measurement campaign in a dense urban environment, using a UWB channel sounder. Measurements were taken with two different antenna heights of 100 cm (representing an upright person [1]) and 10 cm (representing a person or sensor lying on the ground), in LOS and NLOS environments. From the measurements, we extract the channel impulse response (CIR), ranging information and power delay profile (PDP), for each of the environments and antenna heights.

We also study the impact of multiuser interference (MUI) on the ranging accuracy. It is observed that the processing gain of the time-hopping (TH) sequences is not sufficient to suppress the MUI for ranging applications. This is because the first arriving path is not always the strongest path and can have lower energy than the residual MUI, especially in NLOS conditions. We propose a novel coherent ranging algorithm that suppresses the MUI without having to know the TH sequences of the interfering users. Only the TH sequence of the desired user is assumed known to the receiver. The performance of the proposed ranging scheme is evaluated on the measurement data and compared with some well-known thresholding schemes.

The paper is organized as follows. The measurement setup is described in Sec. II. The CIR and range extraction in AWGN channel are given in Sec. III-A. Range extraction in MUI is given in Sec. III-C. Results and Conclusions are given in Sec. IV and Sec. V respectively. The mathematical details are moved to the Appendix.

II. MEASUREMENT SETUP

A. Measurement Site

The measurements were performed for both LOS and NLOS scenarios at the Vivian Hall of Engineering (VHE) building at USC, which is in a dense urban environment. A map of the measurement site, with transmitter and receiver locations, is shown in Figure 1. The LOS measurements were performed in the quad area, which is an open space enclosed by tall buildings and trees on all the four sides, making it a multipath rich environment. The terrain is a flat field mainly made up of 5 cm high grass. The transmitter was fixed and the receiver was moved around. Measurements were carried out with 3 sets of distances between Tx and Rx (20 m, 30 m, and 40 m). For each distance, the receiver was placed at 3 different positions (far apart) along the circumference of the circle with transmitter as the center. At every position, a virtual 1x4 SIMO antenna array, with horizontal separation of 10 cm was used at the
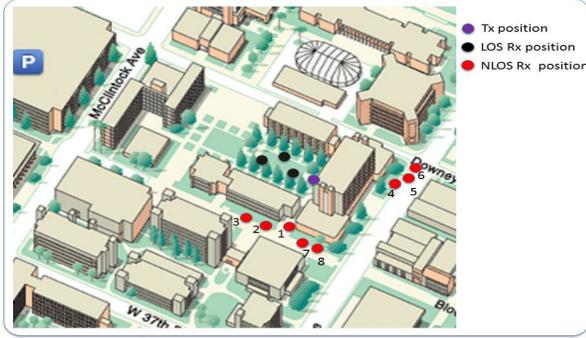
[1]Radio worn on person's hip.

Fig. 1. Floor map of the LOS and NLOS measurements.

receiver to average over the small scale fading. Two sets of measurements were performed, with the Tx/Rx antenna heights both set to 10 cm at first, and later changed to 100 cm for the second measurement.

For the NLOS measurements, the transmitter was fixed and the receiver was moved around the buildings as shown in the figure. The buildings are steel concrete structures. Measurements were taken at eight different receiver positions. The measurement locations has a dense vegetation of height 50 cm. The same virtual array arrangements and height combinations were used as in the LOS measurements.

B. Hardware and Excitation signal

The channel measurement campaign was performed with a UWB channel sounder. The core components are an arbitrary waveform generator (AWG) that can generate signals up to 12 GHz with a sampling rate of 24 GS/s. A digital sampling scope (DSO) operating at 40 GS/s is used at the receiver for data acquisition. The transmitter and receiver were synchronized using a trigger signal transported from the AWG to the DSO using a radio-over-fiber link. A pair of UWB Skycross Omni-directional antennas were used at transmitter and receiver. The transmit chain comprises of antenna, a 10 W, 40 dB power amplifier, a 22 dB gain pre-amplifier and the AWG. The receive chain comprises of antenna, a 30 dB low noise amplifier (LNA) and DSO. The transmitter sends a periodic multitone OFDM-like waveform, with frequency range 3 GHz – 10 GHz. It has a center frequency of 6.5 GHz and 9559 sub carriers with a uniform spacing of 732.42 KHz. Each waveform is 1.36 μs long and we store 50 such waveforms at the DSO for every measurement. We also record 3.45 μs of receiver noise (transmitter off) for every measurement. This is used to compute the noise power, N_0, and to set the parameters during the post processing. More details about the hardware and the excitation signal can be found in [1].

III. POST-PROCESSING

A. AWGN Channels

Since the measurements were conducted close to campus buildings with WiFi access points and devices, there was significant interference. The received signal is thus first passed through a band pass filter to remove the out of band interference. The following parameters are extracted for each of the antenna height combinations:

1) *Impulse response:* A high-resolution CLEAN algorithm [8] is used to extract the channel impulse response from the received waveform. CLEAN is an iterative deconvolution technique, in which the received signal is correlated with the template signal, and the amplitude and location of the correlation peak is determined, followed by a subtraction of the contribution of the thus-detected MPC from the received signal. The residual signal is correlated with the template to determine the next strongest MPC. This process repeats until the strength of the thus-detected MPC falls below a predetermined threshold. The template signal was obtained from a measurement taken with the setup in the anechoic chamber at USC, with a known distance between transmitter and receiver.

2) *Range:* The MPC with the smallest delay is interpreted as corresponding to the (quasi-) LOS component, and thus allowing the extraction of the range information. It can be seen that the choice of threshold determines the ranging accuracy. Two different thresholds are considered. (1) *Genie thresholding:* For every measurement, the threshold is chosen to minimize the instantaneous ranging error. This is done by performing the brute-force Monte Carlo simulations-based search. Since the implementation requires knowledge of the instantaneous ranging error (and thus, of the true location), this is not feasible in practice. (2) *Lookup table thresholding:* The optimal threshold for LOS/NLOS scenarios is computed as follows. For every receiver position, the signal-to-noise ratio (SNR) is computed by averaging over the small scale fading and the Monte Carlo simulations were performed for these parameter settings and with IEEE 802.15.4a CM5 (outdoor LOS)/CM6 (outdoor NLOS) channel models [9]. The correlation threshold with the minimum root mean square error (RMSE) of the range is used.

3) *Power Delay Profile (PDP):* Let $h_k(\tau, p)$ denote the extracted CIR between transmitter and the kth virtual receive antenna, for a specific receiver position p. The squared magnitude of CIR gives the local PDP, which is averaged over the receive antenna measurements to get the average PDP (APDP).

$$APDP(\tau, p) = \frac{1}{4} \sum_{k=1}^{4} |h_k(\tau, p)|^2 . \qquad (1)$$

For each receiver position, the RMS delay spread is computed from the respective APDP.

$$\tau_{rms}(p) = \sqrt{\frac{\int (\tau - \bar{\tau}(p))^2 APDP(\tau, p) d\tau}{\int APDP(\tau, p) d\tau}}.$$

where $\bar{\tau}(p) \triangleq \frac{\int \tau APDP(\tau, p) d\tau}{\int APDP(\tau, p) d\tau}$ is the mean delay spread. $\tau_{rms}(p)$ is further averaged over different receiver positions to get the RMS delay spread of the channel.

B. Simulating TH-IR and MUI

We now study the impact of MUI on the ranging accuracy in TH-IR systems. Since the received waveform is a periodic, multi-tone waveform and only one AWG and DSO was used

in the measurement campaign, the following post-processing is done to simulate the TH-IR systems and the MUI.

Simulating the time-hopping effect: The filtered received signal is divided into $N = 50$ waveforms, each of length $T_f = 1.36$ μs. The time-hopping signal is obtained by introducing a cyclic shift to each of the N waveforms and adding them back together. [2]

Simulating the MUI: MUI is simulated by adding the measurements taken at different receiver positions. Since the transmitter location is same for all the measurements, assuming that the channel is reciprocal, this has the same effect as if multiple users were transmitting at the same time. For instance, $I = 3$ level MUI can be simulated by adding the noisy received waveforms at positions 5, 6 and 7 as interference to the received waveform at position 1. In general, I represents the number of active interfering users. We assume that the receiver only knows the TH sequence of the desired user and not of the interfering users.

C. Range extraction in MUI

Thresholding schemes: The received waveform is de-hopped using the TH sequence of the desired user and CLEAN algorithm is used to extract the range information as described in Sec. III-A2. The lookup table is now a function of SNR, signal-to-interference ratio (SIR) and I. While the processing gain of the TH-IR reduces the MUI, it is often insufficient for range extraction as the (quasi-) LOS component is not always the strongest MPC and can even have lower energy than the residual interference, especially in NLOS conditions. Thus, finding a good correlation threshold for the CLEAN algorithm, to separate the interference MPCs from the LOS component of the desired user is difficult and hence can result in large ranging errors either because of early false alarms from interference MPC or miss detection of signal MPC. We thus employ a new MUI suppression method to improve the performance. We outline here only the fundamental principles; a detailed analysis can be found in [10].

Proposed ranging algorithm to suppress MUI: After de-hopping the received waveform, $r(t)$, the receiver effectively has N waveforms, $\{r^{(n)}(t), 1 \leq n \leq N\}$. Assuming that the channel is quasi-static during the transmission of the ranging signals, the signal MPCs in the N waveforms are time aligned and have the same strength. On the other hand the location of an interference MPC can be different in different waveforms. This is because the difference between the chip sequence of the desired and an interfering user can be different for different waveforms. Thus, we can detect the interference MPCs and remove their contribution from the waveforms before averaging and thereby avoiding the early false alarms from interference. Below are the steps of the algorithm.

1) Impulse response extraction from the waveforms: The Impulse response is extracted from each of the N waveforms using the CLEAN algorithm. A fixed correlation threshold, μ, is used so that the false alarm probability due to the noise is small. If $\{\hat{\alpha}_k, k \geq 1\}$ are the estimated strength of the MPCs and N_0 is the noise power spectral density (PSD), it can be shown that with $\mu = 0.02\sqrt{\sum_k \hat{\alpha}_k^2} + 2.58\sqrt{N_0}$ [3], the false alarm probability from noise is less than 0.01. The details are given in Appendix A.

Let $\left\{\hat{\tau}_k^{(n)}, \hat{\alpha}_k^{(n)}, 1 \leq k \leq L_n\right\}$ be the location and the strength of the MPCs extracted from the waveform $r^{(n)}(t)$. The impulse response is defined as $\hat{h}^{(n)}(t) \triangleq \sum_{k=1}^{L_n} \hat{\alpha}_k^{(n)} \delta(t - \hat{\tau}_k^{(n)})$. The MPC delay $\hat{\tau}_k^{(n)}$ can correspond to contributions from desired user, the interfering users, or a noise peak.

2) Separating the interference and signal MPCs: Consider the set $\left\{\hat{h}^{(n)}(\tau), 1 \leq n \leq N\right\}$. If τ corresponds to a signal MPC location, most of the values in the set are similar. If τ corresponds to an interference MPC location in one waveform, some of the values in the remainder of the set will be zero and even the non-zero values in the set are distinct. Also, the odds of noise peaks happening at the same location in multiple waveforms are low. We can use these facts to distinguish desired signal components from interference and noise. However, we also have to take into account that because of noise, the estimated MPC locations can vary around their true locations. With high probability the estimate in N waveforms will all lie in the interval $[\tau - W, \tau + W]$, where τ is the true signal MPC location. Intuitively, the faster the decay of the auto-correlation function of the template, the smaller is the W.

Using the intuition presented above, we propose the following heuristic rule to decide if the MPC location $\hat{\tau}_k^{(n)}$ correspond to signal MPC or interference/noise MPC. We do not distinguish between interference MPC and noise peak.

For $1 \leq n \leq N$ and $1 \leq k \leq L_n$,

- Construct the set $\{X_n, 1 \leq n \leq N\}$, where $X_n \triangleq \int_{w=-W}^{W} \hat{h}^{(n)}(\hat{\tau}_k^{(n)} - w)dw$. Let M be the number of non-zero values in this set.
- $M < \bar{N}$: Declare $\hat{\tau}_k^{(n)}$ as an interference MPC (A signal MPC will be detected in at least $\bar{N}$ out of N waveforms). $\bar{N}$ is an algorithm parameter.
- $M \geq \bar{N}$: If $\hat{\tau}_k^{(n)}$ is an interference MPC, these M data points are distinct and far apart. If it is a signal MPC, most of these data points are clustered. [4] $\hat{\tau}_k^{(n)}$ is declared as signal MPC if there exists a cluster of at least $\bar{N}$ data points around X_k. Otherwise, it is declared as interference MPC.

3) Interference suppression and noise averaging: The contribution of the thus-detected interference MPCs is removed from each of the waveforms.

---

[2]Cyclic shift is required to make sure that the interference CIR in N waveforms differs only by a time shift. Since the transmitted signal is a long multitone waveform, a linear shift would result in totally distinct CIR for interference in the N waveforms.

[3]Starting with $\mu = 2.58\sqrt{N_0}$, it is updated every iteration.

[4]In some of the waveforms, an interference MPC can overlap with the signal MPC thereby deteriorating the MPC amplitude estimate.
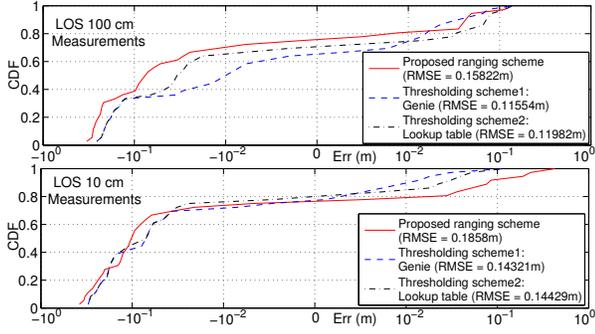
Fig. 2. Ranging error in LOS AWGN environment.

Fig. 3. Ranging error in NLOS AWGN environment.

Fig. 4. NLOS measurement map of USC VHE quad.

Let $\Delta_n^I \triangleq \left\{ \hat{\tau}_k^{(n)}, 1 \le k \le L_n \mid \hat{\tau}_k^{(n)} \text{is interference/noise MPC} \right\}$. The refined signal is

$$\tilde{r}^{(n)}(t) = r^{(n)}(t) - \sum_{\tau \in \Delta_n^I} \hat{h}^{(n)}(\tau) p(t - \tau), \; 1 \le n \le N,$$

where $p(t)$ is the UWB pulse (or) template signal used by all the users. The waveforms are now averaged to suppress the residual interference and noise.

4) Range extraction: The impulse response is extracted from the averaged waveform using CLEAN. Let $\{\hat{\alpha}_l, \hat{\tau}_l, l \ge 1\}$ be the extracted MPCs. Similar to the arguments presented in Appendix A, the correlation threshold of $\mu = 0.02\sqrt{\sum_{n=1}^{N}\sum_{\tau \in \Delta_n^I} \frac{1}{N^2}(\hat{h}^{(n)}(\tau))^2 + \sum_l \hat{\alpha}_l^2} + \eta\sqrt{N_0}$ is used. Here η is a parameter that determines the probability of false alarm from noise. It is taken from the lookup table generated for CM5/CM6 channel models with $I = 0$ (no interference).

We furthermore require that the delay between the first and second MPC is consistent with the statistics of the inter-arrival times of MPCs. This is required to filter out any residual interference MPCs, as their inter-arrival times has significantly larger delays than the signal MPCs. When the MPC arrival times are modeled as Poisson process with parameter λ, the probability that the inter-arrival times exceed $\frac{5.3}{\lambda}$ is 0.5%. Hence, the time-of-arrival (ToA) or range estimate is

$$\widehat{\text{ToA}} = \min\left\{\hat{\tau}_k : |\hat{\tau}_k - \hat{\tau}_{k+1}| < \frac{5.3}{\lambda}\right\}, \qquad (2)$$

λ is computed from the APDP of the channel.

IV. RESULTS

In this section, we present the range estimates as extracted with our proposed scheme, and compare them with the thresholding scheme. All of these schemes are applied to our measured LOS and NLOS channels. For the proposed ranging scheme, $W = 0.5R_p^{-1}(0.4)$ ($R_p(.)$ is the auto-correlation function of the template signal.) is used. $\bar{N} = 0.02WN$ and $\bar{N} = \frac{N}{2}$ are used for AWGN and MUI respectively. More discussion on the choice of parameters can be found in [10]. We first present the results with the AWGN channel, and then with the MUI.

A. Ranging error in AWGN

Figure 2 and 3 respectively plots the cumulative distribution function (CDF) of the ranging error $(\hat{d} - d)$, for the LOS and
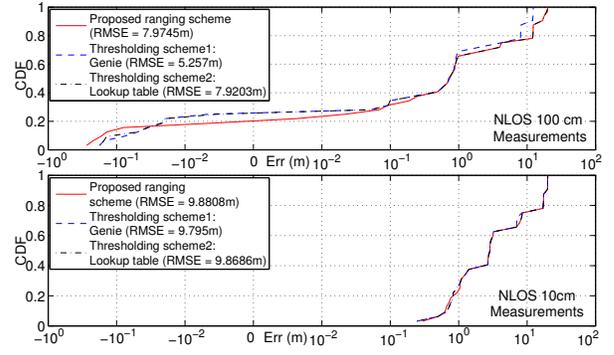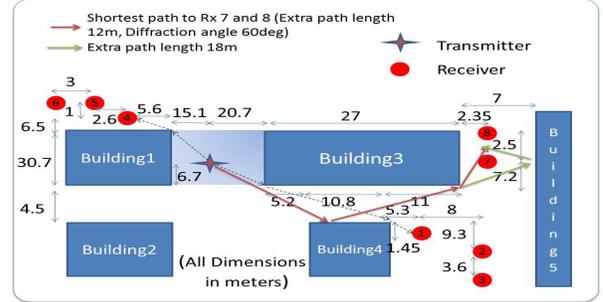
NLOS measurements, taken with two different antenna heights of 10 cm and 100 cm. While the proposed ranging scheme is as good as lookup table thresholding scheme in NLOS conditions, it has slightly higher RMSE in LOS conditions. The genie thresholding outperforms the other two schemes in AWGN channel.

While the RMSE of the LOS measurements is 12 cm, it is several meters for the NLOS measurements. The large ranging errors for the NLOS measurements can be better understood from the map in Figure 4. For these receiver locations, the direct path is completely blocked by buildings. The only viable signal paths are diffractions around the corners of the buildings and reaching the receiver as shown. While the ranging errors for the measurements taken at receiver positions 1–6 was less than 5 m, it was 18–20 m for receiver positions 7 and 8. As shown in the figure, for the receiver positions 7 and 8, the shortest measurable signal path is the reflection from building 4, followed by diffraction at building 3. This path length is 12 m larger than the Euclidean distance between transmitter and receiver. However, the diffraction angle at building 3 is 60 degrees. Hence, the ray undergoes significant loss from diffraction and the corresponding MPC is not detectable. The next shortest path is from double reflection at buildings 4 and 5 as shown in Figure 4. This path length is 18 m larger than the Euclidean distance. If we excluded receiver positions with such large errors (*i.e.*, restrict our evaluations to receiver locations 1–6), the RMSE with the proposed ranging scheme is 1.34 m and 3.5 m respectively for antenna height of 100 cm and 10 cm.

Also, from Figure 2 and 3 it can be seen that the RMSE increases when the antennas are closer to the ground and the increase is more pronounce for NLOS scenario. Since
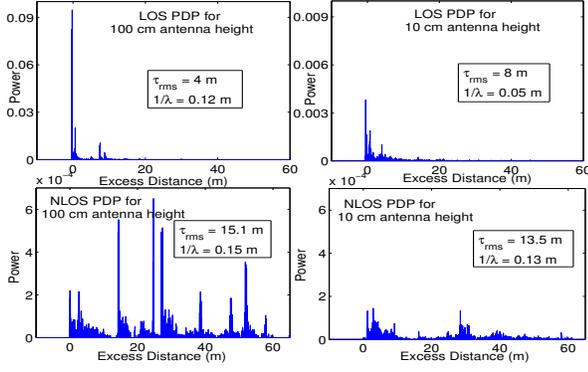
Fig. 5. APDP for NLOS and LOS scenarios for different antenna heights.

the ranging error mainly depends on the strength of the LOS component, this behavior can be better understood from the APDP of the respective channels. Figure 5 plots the APDP of LOS and NLOS channels for receiver at position 7. Consider the LOS scenario in which the majority of the energy is concentrated at the LOS component. For 100 cm antenna heights, the LOS component is isolated and hence can be separated from the next arriving MPCs. For 10 cm antenna heights, because of the proximity to the ground the LOS component is close to the next arriving MPCs and have comparable energy, thus increasing the ranging error. Consider the NLOS scenario. Since the measurement locations has a rich vegetation of height 50 cm, some of the strong MPCs are missing when the antenna height is reduced from 100 cm to 10 cm. Also, the energy in the first arriving path is reduced. Both of these can result in increased ranging errors. The RMS delay spread (τ_{rms}) and the average inter-arrival times between the MPCs ($1/\lambda$) are given for each of the channels.

Under similar parameter settings like SNR and bandwidth, the performance was evaluated with IEEE 802.15.4a channel models. With CM5 (outdoor LOS) channel model, $\tau_{rms} = 6$ m and RMSE $= 0.1$ m, and agrees well with the corresponding numbers extracted from the LOS measurements. With CM6 (outdoor NLOS) channel model, $\tau_{rms} = 25$ m and RMSE < 1 m, and are significantly different from the corresponding numbers extracted from the NLOS measurements. These channel models assume that the LOS component is always detected albeit with low SNR. However, as described earlier, in NLOS scenarios, the LOS component can be completely blocked for some receiver locations.

B. Ranging error in MUI

We now study the impact of MUI on the ranging error. The performance of the proposed ranging scheme is evaluated with the measurement data, and compared with the thresholding schemes. The Energy based nonlinear filtering schemes in Ref. [6] suffer from poor SNR and hence the corresponding performance curves are not shown for want of space.

Figure 6 and 7 compares the CDF of the ranging error, for different ranging schemes, when both the desired user and interfering users are in a LOS scenario. Results are shown for $I = 1$ and $I = 5$, for two different antenna heights. Note that I is the number of interfering users. It can be seen that the
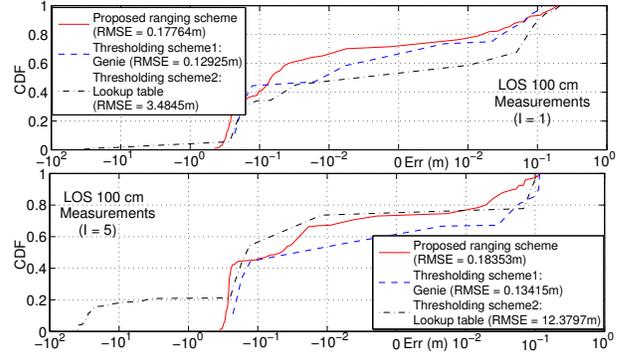

Fig. 6. Ranging error with MUI in LOS scenario for 100 cm antenna height.
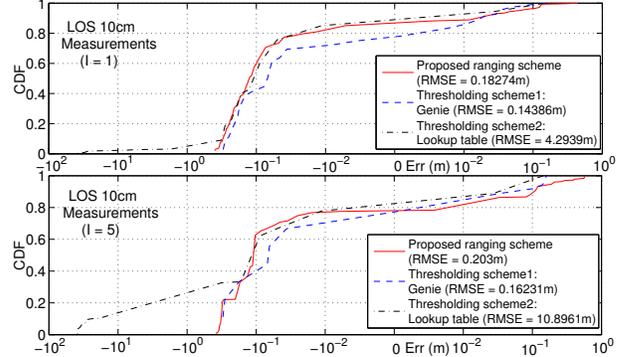

Fig. 7. Ranging error with MUI in LOS scenario for 10 cm antenna height.

proposed ranging scheme gives significantly lower RMSE than the lookup table thresholding scheme. While the ranging error with the proposed scheme is always less than 0.5 m, it is more than 20 m for 10% of times with the lookup table thresholding scheme when $I = 5$. While the proposed scheme is robust to the number of interfering users, the performance with the lookup table thresholding scheme degrades as I increases. Genie thresholding outperforms the other two ranging schemes in this case. As earlier, the RMSE slightly increases when the antennas are closer to the ground.

Similar observations hold even for NLOS measurements. Figure 8 and 9 compares the CDF of the ranging error for different ranging schemes, when both the desired user and interfering users are in the NLOS scenario. Since the RMSE is dominated by receiver positions 7 and 8, we exclude the corresponding measurements for the performance comparison of different ranging schemes. The impact of antenna height and MUI on the ranging error is more significant in NLOS scenarios and even the genie thresholding scheme cannot suppress the MUI effectively.

V. CONCLUSIONS

We carried out a UWB range measurement campaign in a dense urban environment, with two different antenna heights. We observed that the RMSE in the range increased from 0.12 m to 0.14 m for LOS measurements and from 7.9 m to 9.8 m for NLOS measurements, when the antenna height reduced from 100 cm to 10 cm. In LOS environment, the measured RMSE is consistent with IEEE 802.15.4a CM5 channel model. However, the measured RMSE in NLOS environment is much higher than the RMSE obtained with CM6
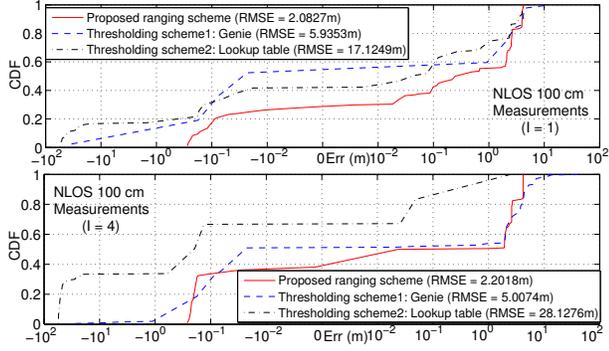
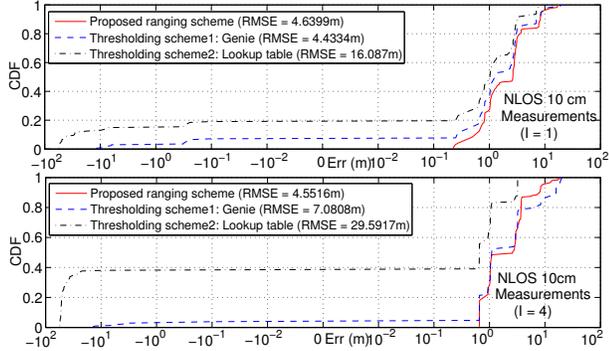Fig. 8. Ranging error with MUI in NLOS scenario for 100 cm antenna height.

Fig. 9. Ranging error with MUI in NLOS scenario for 10 cm antenna height.

channel model, under similar parameter settings. These values are orders of magnitude higher than often reported for UWB ranging. Their validity has been confirmed not only through a careful testing of the measurement setup, and evaluation by at least three independent algorithms, but also by physical explanations of the results. It is also noteworthy that these much larger errors have a significant impact on the design of UWB localization systems: very large errors are unavoidable for certain Tx/Rx pairs, so that accurate localization requires redundancy in the measurements and network localization techniques that take possibly large errors into account.

A further observation was that the processing gain of TH sequences is not sufficient to suppress the MUI for ranging applications. We thus proposed a novel coherent ranging algorithm to mitigate the MUI and showed that it is robust to the number of interfering users and can even outperform the genie-aided thresholding schemes in some scenarios.

APPENDIX

A. False alarm from noise

Let $y(t) = \sum_{k=1}^{L} \alpha_k p(t - \tau_k) + n(t)$ be the real valued received signal in a multipath channel with $p(t)$ and $n(t)$ being the unit energy template signal and the noise with variance N_0 respectively. Let $\{\hat{\alpha}_1, \cdots, \hat{\alpha}_L, \hat{\tau}_1, \cdots, \hat{\tau}_L\}$ be the location and strength of the L strongest MPCs extracted using CLEAN. The residual signal after L iterations is $y^{(L)}(t) = \sum_{k=1}^{L} \alpha_k p(t - \tau_k) - \sum_{k=1}^{L} \hat{\alpha}_k p(t - \hat{\tau}_k) + n(t)$. The correlation between the template and the residual signal is $\rho(\tau) = \sum_{k=1}^{L} \alpha_k R_p(\tau - \tau_k) - \sum_{k=1}^{L} \hat{\alpha}_k R_p(\tau - \hat{\tau}_k) + N(\tau)$. Here $N(\tau) \triangleq \int n(t)p(t - $

Fig. 10. Autocorrelation function of the template signal.

$\tau)dt$ is a zero-mean real Gaussian RV with variance N_0. $R_p(\tau)$ is the autocorrelation of the template signal and is shown in Figure 10. For $|\alpha_k| >> N_0$, we have $\hat{\alpha}_k \approx \alpha_k$.

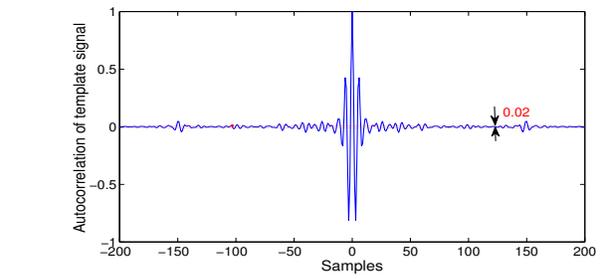Let τ be a noise only region. Because of the ripples in the correlation floor [5], even a small error in the MPC location estimates can result in $\hat{\alpha}_k (R_p(\tau - \tau_k) - R_p(\tau - \hat{\tau}_k))$ comparable to N_0. From Figure 10, the amplitude of the ripple is approximately 0.02 and hence we approximate $\left| \sum_{k=1}^{L} \alpha_k R_p(\tau - \tau_k) - \sum_{k=1}^{L} \hat{\alpha}_k R_p(\tau - \hat{\tau}_k) \right|$ with $0.02\sqrt{\sum_{k=1}^{L} \hat{\alpha}_k^2}$.

CLEAN makes false detection of τ as a signal MPC, if $|\rho(\tau)| > \mu$. Using the above approximation it is easy to see that for $\mu = 0.02\sqrt{\sum_k \hat{\alpha}_k^2} + 2.58\sqrt{N_0}$, the probability of false alarm from noise peak is less than 0.01.

REFERENCES

[1] S. Sangodoyin, S. Niranjayan and A. F. Molisch, "Ultrawideband Near-Ground Outdoor Propagation Channel Measurements and Modeling," *in Proc. 7th EuCAP*, Gothenburg, Sweden. April 2013.
[2] D. Dardari, A. Conti, U. Ferner, A. Giorgetti, M. Z. Win, "Ranging With Ultrawide Bandwidth Signals in Multipath Environments," *Proc. of the IEEE*, vol.97, no.2, pp.404–426, Feb. 2009.
[3] B. Alavi, N. Alsindi and K. Pahlavan, "UWB Channel Measurements for Accurate Indoor Localization," *Proc. IEEE Military Commun. Conf. (MILCOM)*, 2006.
[4] G. Bellusci, G. J. M. Janssen, J. Yan and C. C. J. M. Tiberius, "Model of Distance and Bandwidth Dependency of TOA-Based UWB Ranging Error," *Proc. IEEE Int. Conf. Ultra-Wideband (ICUWB)*, vol. 3, pp.193–196, 2008.
[5] C. C. Chong, F. Watanabe and M. Z. Win, "Effect of Bandwidth on UWB Ranging Error," *Proc. IEEE Wireless Commun. and Netw. Conf. (WCNC)*, pp.1559–1564. Mar. 2007.
[6] Z. Sahinoglu and I. Guvenc, "Multiuser interference mitigation in noncoherent UWB ranging via nonlinear filtering," *EURASIP J. Wireless Commun. Netw.*, pp.1–10 2006.
[7] P. Richardson and D. Shan, "Experimental Data Collection and Performance Analysis of Outdoor UWB Positioning System under Static and Mobile Conditions," *EURASIP J. Wireless Commun. Netw.*, pp.1–13 2009.
[8] R. J. M.Cramer, R. A. Scholtz, M. Z. Win, "Evaluation of an Ultrawide-Band Propagation channel," *IEEE Transactions on Antenna and Propagation*, Vol.50, no.5, pp.561–570, May 2002.
[9] A. F. Molisch, D. Cassioli, C. C. Chong, S. Emami, A. Fort, B. Kannan, J. Karedal, J. Kunisch, H. G. Schantz, K. Siwiak, and M. Z. Win, "A comprehensive standardized model for ultrawideband propagation channels," *IEEE Transactions on Antennas and Propagation*, vol. 54, no. 11, pp. 3151–3166, November 2006.
[10] V. Kristem, A. F. Molisch, S. Niranjayan, and S. Sangodoyin, "Coherent UWB ranging in presence of MUI", *submitted to IEEE Trans. Wireless Comm.*

[5] Since $p(t)$ is a long multitone waveform, the autocorrelation has non-zero floor. The ripples in the correlation floor are caused by the non-idealities of the filters in the Tx and Rx chain.